

PUGeo-Net: A Geometry-centric Network for 3D Point Cloud Upsampling

Yue Qian Junhui Hou Sam Kwong

Department of Computer Science

City University of Hong Kong

{yueqian4-c, jh.hou, cssamk}@cityu.edu.hk

Ying He

School of Computer Science and Engineering

Nanyang Technological University

yhe@ntu.edu.sg

Abstract

This paper addresses the problem of generating uniform dense point clouds to describe the underlying geometric structures from given sparse point clouds. Due to the irregular and unordered nature, point cloud densification as a generative task is challenging. To tackle the challenge, we propose a novel deep neural network based method, called PUGeo-Net, that learns a 3×3 linear transformation matrix \mathbf{T} for each input point. Matrix \mathbf{T} approximates the augmented Jacobian matrix of a local parameterization and builds a one-to-one correspondence between the 2D parametric domain and the 3D tangent plane so that we can lift the adaptively distributed 2D samples (which are also learned from data) to 3D space. After that, we project the samples to the curved surface by computing a displacement along the normal of the tangent plane. PUGeo-Net is fundamentally different from the existing deep learning methods that are largely motivated by the image super-resolution techniques and generate new points in the abstract feature space. Thanks to its geometry-centric nature, PUGeo-Net works well for both CAD models with sharp features and scanned models with rich geometric details. Moreover, PUGeo-Net can compute the normal for the original and generated points, which is highly desired by the surface reconstruction algorithms. Computational results show that PUGeo-Net, the first neural network that can jointly generate vertex coordinates and normals, consistently outperforms the state-of-the-art in terms of accuracy and efficiency for upsampling factor $4 \sim 16$.

1. Introduction

Three-dimensional (3D) point clouds, as the raw representation of 3D data, are used in a wide range of applications, such as 3D immersive telepresence [2], 3D city reconstruction [3], [4], cultural heritage reconstruction [5], [6], geophysical information systems [7], [8], autonomous driving [9], [10], simultaneous localization and mapping [11], [12], and virtual/augmented reality [13], [14], just to name a few. Though recent years have witnessed great progress on the 3D sensing technology [15], [16], it is

still costly and time-consuming to obtain dense and highly detailed point clouds, which are beneficial to the subsequent applications. Therefore, amendment is required to speed up the deployment of such data modality.

In this paper, instead of relying on the development of hardware, we are interested in the problem of computational based point cloud upsampling: given a sparse, low-resolution point cloud, generate a uniform and dense point cloud with a typical computational method to faithfully represent the underlying surface. Since the problem is the 3D counterpart of image super-resolution [17], [18], a typical idea is to borrow the powerful techniques from the image processing community. However, due to the unordered and irregular nature of point clouds, such an extension is far from trivial, especially when the underlying surface has complex geometry.

The existing methods for point cloud upsampling can be roughly classified into two categories: optimization-based methods and deep learning based methods. The optimization methods [19], [20], [21], [22], [23] usually fit local geometry and work well for smooth surfaces with less features. However, these methods struggle with multi-scale structure preservation. The deep learning methods can effectively learn structures from data. Representative methods are PU-Net [24], EC-Net [25] and MPU [26]. PU-Net extracts multi-scale features using point cloud convolution [27] and then expands the features by replication. With additional edge and surface annotations, EC-Net improves PU-Net by restoring sharp features. Inspired by image super-resolution, MPU upsamples points in a progressive manner, where each step focuses on a different level of detail. PU-Net, EC-Net and MPU operate on patch level, therefore, they can handle high-resolution point sets. Though the deep learning methods produce better results than the optimization based methods, they are heavily motivated by the techniques in the image domain and takes little consideration of the geometries of the input shape. As a result, various artifacts can be observed in their results. It is also worth noting that all the existing deep learning methods generate points only, none of them is able to estimate the normals of the original and generated points.

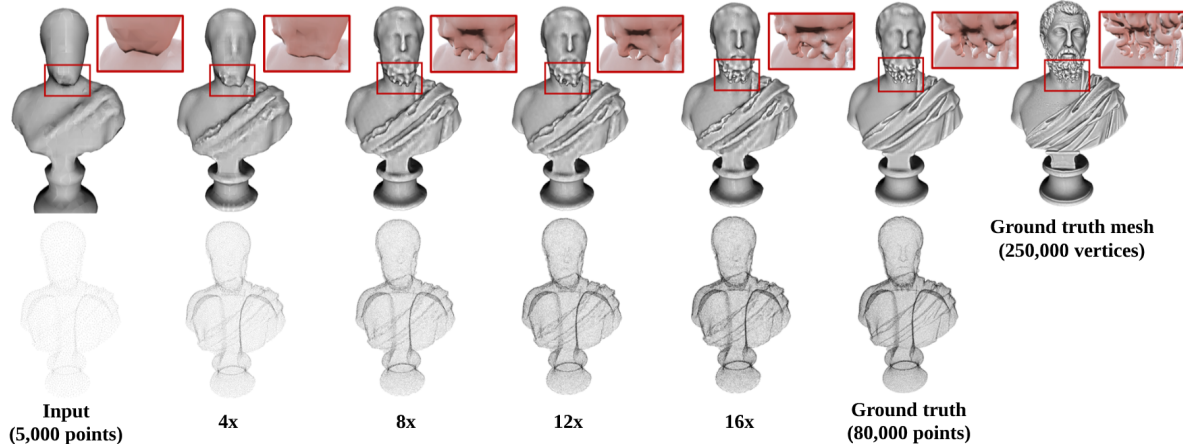


Figure 1: Illustration of various sampling factors of the Rethour Statue model with 5,000 points. Due to the low-resolution input, the details, such as cloth wrinkles and facial features, are missing. PUGeo-Net can effectively generate up to $16\times$ points to fill in the missing part. See also the accompanying video and results.

In this paper, we propose a novel network, called PUGeo-Net, to overcome the limitations in the existing deep learning methods. Our method learns a local parameterization for each point and its normal direction. In contrast to the existing neural network based methods that generate new points in the abstract feature space and map the samples to the surface using decoder, PUGeo-Net performs the sampling operations in a pure geometric way. Specifically, it first generates the samples in the 2D parametric domain and then lifts them to 3D space using a linear transformation. Finally, it warps the tangent plane to obtain 3D points on the curved surface. Through extensive evaluation on commonly used as well as new metrics, we show that PUGeo-Net consistently outperforms the state-of-the-art in terms of accuracy and efficiency for upsampling factors $4 \sim 16\times$. It is also worth noting that PUGeo-Net is the first neural network that can generate dense point clouds with accurate normals, which are highly desired by the existing surface reconstruction algorithms. We demonstrate the efficacy of PUGeo-Net on both CAD models with sharp features and scanned models with rich geometric details and complex topologies. Figure 1 demonstrates the effectiveness of PUGeo-Net on the *Rethour* Statue model.

The main contributions of this paper are summarized as follows.

1. We propose PUGeo-Net, a novel geometric-centric neural network, which carries out a sequence of geometric operations, such as computing the first-order approximation of local parameterization, adaptive sampling in the parametric domain, lifting the samples to the tangent plane, and projection to the curved surface.
2. PUGeo-Net is the first upsampling network that can jointly generate coordinates and normals for the densified point clouds. The normals benefit many down-

stream applications, such as surface reconstruction and shape analysis.

3. We evaluate PUGeo-Net on both synthetic and real-world models and show that PUGeo-Net significantly outperforms the state-of-the-art methods in terms of accuracy and efficiency for all upsampling factors.

2. Related Work

Optimization based methods. Alexa *et al.* [19] interpolated points of Voronoi diagram, which is computed in the local tangent space. Lipman *et al.* developed a method based on locally optimal projection operator (LOP) [20]. It is a parametrization-free method for point resampling and surface reconstruction. Subsequently, the improved weighted LOP and continuous LOP were developed by Huang *et al.* [21] and Preiner *et al.* [22] respectively. These methods assume that points are sampling from smooth surfaces, which degrades upsampling quality towards sharp edges and corners. Huang *et al.* [23] presented an edge-aware (EAR) approach which can effectively preserve the sharp features. With given normal information, EAR algorithm first resamples points away from edges, then progressively upsamples points to approach the edge singularities. However, the performance of EAR heavily depends on the given normal information and parameter tuning. In conclusion, point cloud upsampling methods based on geometric priors either assume insufficient hypotheses or require additional attributes.

Deep learning based methods. The deep learning based upsampling methods first extract point-wise feature via point clouds CNN. The lack of point order and regular structure impede the extension of powerful CNN to point clouds. Instead of converting point clouds to other data representations like volumetric grids [28], [29], [30] or graphs [31], [32], recently the point-wise 3D CNN [33],

[34], [27], [35], [36] successfully achieved state-of-the-art performance for various tasks. Yu *et al.* pioneered PU-Net[24], the first deep learning algorithm for point cloud upsampling. It adopts PointNet++ [27] to extract point features and expands features by multi-branch MLPs. It optimizes a joint reconstruction and repulsion loss function to generate point clouds with uniform density. PU-Net surpasses the previous optimization based approaches for point cloud upsampling. However, as it does not consider the spatial relations among the points, there is no guarantee that the generated samples are uniform. The follow-up work, EC-Net [25], adopts a joint loss of point-to-edge distance, which can effectively preserve sharp edges. EC-Net requires labelling the training data with annotated edge and surface information, which is tedious to obtain. Wang *et al.* [26] proposed a patch-based progressive upsampling method (MPU). Their method can successfully apply to large upsampling factor, say $16\times$. Inspired by the image super-resolution techniques, they trained a cascade of upsampling networks to progressively upsample to the desired factor, with the subnet only deals with $2\times$ case. MPU replicates the point-wise features and separates them by appending a 1D code $\{-1, 1\}$, which does not consider the local geometry. MPU requires a careful step-by-step training, which is not flexible and fails to gain a large upsampling factor model directly. Since each subnet upsizes the model by a factor 2, MPU only works for upsampling factor which is a power of 2. PUGeo-Net distinguishes itself from the other deep learning method from its geometry-centric nature. See Sec. 4 for quantitative comparisons and detailed discussions.

3. Proposed Method

3.1. Motivation & Overview

Given a sparse point cloud $\mathcal{X} = \{\mathbf{x}_i \in \mathbb{R}^{3 \times 1}\}_{i=1}^M$ with M points and the user-specified upsampling factor R , we aim to generate a dense, uniformly distributed point cloud $\mathcal{X}_R = \{\mathbf{x}_i^r \in \mathbb{R}^{3 \times 1}\}_{i,r=1}^{M,R}$, which contains more geometric details and can approximate the underlying surface well. Similar to other patch-based approaches, we first partition the input sparse point cloud into patches via the farthest point sampling algorithm, each of which has N points, and PUGeo-Net processes the patches separately.

As mentioned above, the existing deep learning based methods are heavily built upon the techniques in 2D image domain, which generate new samples by replicating feature vectors in the abstract feature space, and thus the performance is limited. Moreover, due to little consideration of shape geometry, none of them can compute normals, which play a key role in surface reconstruction. In contrast, our method is motivated by parameterization-based surface resampling, consisting of 3 steps: first it parameterizes a 3D surface S to a 2D domain, then it samples in the parametric

domain and finally maps the 2D samples to the 3D surface. It is known that parameterization techniques depend heavily on the topology of the surface. There are two types of parameterization, namely local parameterization and global parameterization. The former deals with a topological disk (i.e., a genus-0 surface with 1 boundary) [38]. The latter works on surfaces of arbitrary topology by computing canonical homology basis, through which the surface is cutting into a topological disk, which is then mapped to a 2D domain [39]. Global constraints are required in order to ensure the parameters are continuous across the cuts [37].

In our paper, the input is a point cloud sampled from a 3D surface of arbitrary topology. Since computing and learning a global parameterization is expensive, our idea is to learn a simplified local parameterization for each point. Let us parameterize a local neighborhood of point \mathbf{x}_i to a 2D domain via a differential map $\Phi: \mathbb{R}^2 \rightarrow \mathbb{R}^3$ so that $\Phi(0, 0) = \mathbf{x}_i$ (see Figure 3). The Jacobian matrix $\mathbf{J}_\Phi = [\Phi_u, \Phi_v]$ provides the best first-order approximation of the map $\Phi: \Phi(u, v) = \Phi(0, 0) + [\Phi_u, \Phi_v] \cdot (u, v)^T + O(u^2 + v^2)$, where Φ_u and Φ_v are the partial derivatives. The normal of point \mathbf{x}_i can be computed by the cross product $\mathbf{n}_i = \Phi_u(0, 0) \times \Phi_v(0, 0)$. It is easy to verify that the point $\hat{\mathbf{x}} \triangleq \mathbf{x}_i + \mathbf{J}_\Phi \cdot (u, v)^T$ is on the tangent plane of \mathbf{x}_i , since $(\hat{\mathbf{x}} - \mathbf{x}_i) \cdot \mathbf{n}_i = 0$. In our method, we use the augmented Jacobian matrix $\mathbf{T} = [\Phi_u, \Phi_v, \Phi_u \times \Phi_v]$ to compute the normal $\mathbf{n}_i = \mathbf{T} \cdot (0, 0, 1)^T$ and the point $\hat{\mathbf{x}} = \mathbf{x}_i + \mathbf{T} \cdot (u, v, 0)^T$. Matrix \mathbf{T} is of full rank if the surface is regular at \mathbf{x}_i .

With the linear transformation matrix \mathbf{T}_i learned for each point \mathbf{x}_i , PUGeo-Net proceeds as follows: it generates new samples $\{(u_i^r, v_i^r)\}_{r=1}^R$ in the 2D parametric domain. Then it computes the normal $\mathbf{n}_i = \mathbf{T}_i \cdot (0, 0, 1)^T$. After that, it maps each generated 2D sample (u_i, v_i) to the tangent plane of \mathbf{x}_i by $\hat{\mathbf{x}}_i^r = \mathbf{T}_i \cdot (u_i^r, v_i^r, 0)^T + \mathbf{x}_i$. Finally, it projects $\hat{\mathbf{x}}_i^r$ to the curved 3D surface by computing a displacement δ_i^r along the normal direction.

Fig. 2(b) illustrates the network architecture of PUGeo-Net, which consists of hierarchical feature extraction and recalibration (Sec 3.2), parameterization-based point expansion (Sec 3.3) and coordinate and normal refinement (Sec 3.4). We adopt a joint loss function to guide the prediction of vertex coordinates and normals (Sec 3.5).

3.2. Hierarchical Feature Learning and Recalibration

To handle the rotation-invariant challenge of 3D point clouds, we adopt an STN-like mini-network [40], which computes a global 3D transformation matrix $\mathbf{A} \in \mathbb{R}^{3 \times 3}$ applied to all points. After that, we apply DGCNN [34] - the state-of-the-art method for point cloud classification and segmentation - to extract hierarchical point-wise features, which are able to encode both local and global intrinsic geometry information of an input patch.

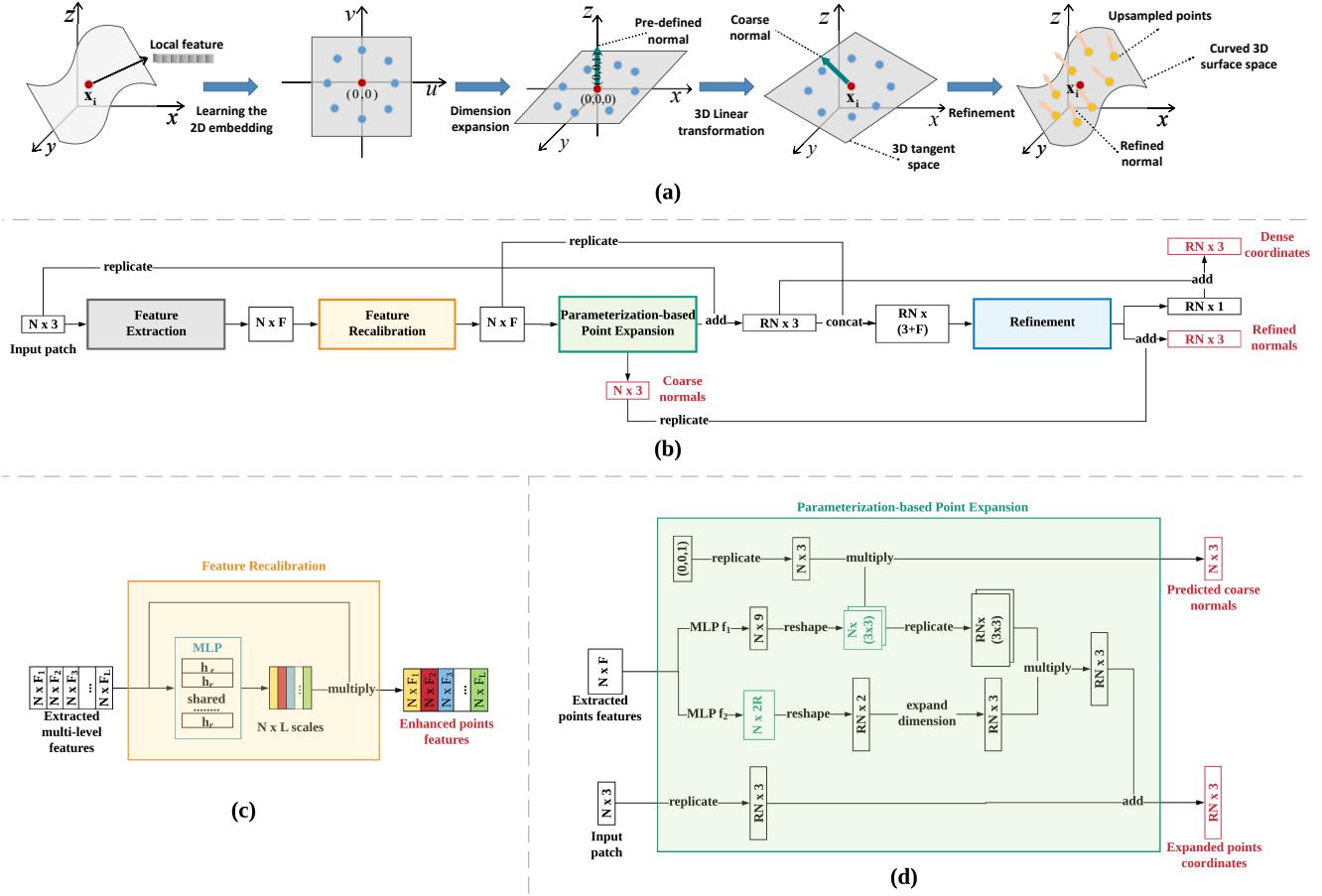


Figure 2: Overview. The top row illustrates the stages of PUGeo-Net: learning local parameterization, point expansion and vertex coordinates and normals refinement. The middle row shows the end-to-end network structure of PUGeo-Net. The output is colored in red. The bottom row shows the details of two core modules: feature recalibration and point expansion.

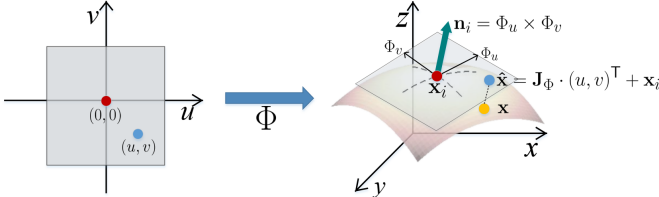


Figure 3: Surface parameterization and its first-order approximation. The local neighborhood of \mathbf{x}_i is parameterized to a 2D rectangular domain via a differentiable map $\Phi: \mathbb{R}^2 \rightarrow \mathbb{R}^3$. The Jacobian matrix $\mathbf{J}_\Phi(0,0)$ provides the best linear approximation of Φ at \mathbf{x}_i , which maps (u, v) to a point $\hat{\mathbf{x}}$ on the tangent plane of \mathbf{x}_i .

The hierarchical feature learning module extracts features from low- to high-levels. Intuitively speaking, as the receptive fields increase, skip-connection [41], [42], [43], a widely-used technique in 2D vision task for improving the feature quality and the convergence speed, can help preserve details in all levels. To this end, as illustrated in Fig. 2(c), instead of concatenating the obtained features directly, we perform feature re-calibration by a self-gating

unit [44], [45] to enhance them, which is computationally efficient.

Let $\mathbf{c}_i^l \in \mathbb{R}^{F_l \times 1}$ be the extracted feature for point \mathbf{x}_i at the l -th level ($l = 1, \dots, L$), where F_l is the feature length. We first concatenate the features of all L layers, i.e., $\hat{\mathbf{c}}_i = \text{Concat}(\mathbf{c}_i^1, \dots, \mathbf{c}_i^L) \in \mathbb{R}^F$, where $F = \sum_{l=1}^L F_l$ and $\text{Concat}(\cdot)$ stands for the concatenation operator. The direct concatenate feature is passed to a small MLP $h_r(\cdot)$ to obtain the logits $\mathbf{a}_i = (a_i^1, a_i^2, \dots, a_i^L)$, i.e.,

$$\mathbf{a}_i = h_r(\hat{\mathbf{c}}_i), \quad (1)$$

which are further fed to a softmax layer to produce the recalibration weights $\mathbf{w}_i = (w_i^1, w_i^2, \dots, w_i^L)$ with

$$w_i^l = \frac{e^{a_i^l}}{\sum_{k=1}^L e^{a_i^k}}. \quad (2)$$

Finally, the recalibrated multi-scale features are represented as the weighted concatenation:

$$\mathbf{c}_i = \text{Concat}(w_i^1 \cdot \mathbf{c}_i^1, w_i^2 \cdot \mathbf{c}_i^2, \dots, w_i^L \cdot \mathbf{c}_i^L). \quad (3)$$

3.3. Parameterization-based Point Expansion

In this module, we expand the input sparse point cloud R times to generate a coarse dense point cloud as well as the

corresponding coarse normals by regressing the obtained multi-scale features. Specifically, the expansion process is composed of two steps, i.e., learning an adaptive sampling in the 2D parametric domain and then projecting it onto the 3D tangent space by a learned linear transformation.

Adaptive sampling in the 2D parametric domain. For each point \mathbf{x}_i , we apply an MLP $f_1(\cdot)$ to its local surface feature \mathbf{c}_i to reconstruct the 2D coordinates (u_i^r, v_i^r) of R sampled points, i.e.,

$$\{(u_i^r, v_i^r) | r = 1, 2, \dots, R\} = f_1(\mathbf{c}_i). \quad (4)$$

With the aid of its local surface information encoded in \mathbf{c}_i , it is expected that the self-adjusted 2D parametric domain maximizes the uniformity over the underlying surface.

Remark. Our sampling strategy is fundamentally different from the existing deep learning methods. PU-Net generates new samples by replicating features in the feature space, and feed the duplicated features into independent multi-branch MLPs. It adopts an additional repulsion loss to regularize uniformity of the generated points. MPU also replicates features in the feature space. It appends additional code +1 and -1 to the duplicated feature copies in order to separate them. Neither PU-Net nor MPU considers the spatial correlation among the generated points. In contrast, our method expands points in the 2D parametric domain and then lifts them to the tangent plane, hereby in a more geometric-centric manner. By viewing the problem in the mesh parametrization sense, we can also regard appending 1D code in MPU as a *predefined* 1D parametric domain. Moreover, the predefined 2D regular grid is also adopted by other deep learning based methods for processing 3D point clouds, e.g., FoldingNet [46], PPF-FoldNet [47] and PCN [48]. Although the predefined 2D grid is regularly distributed in 2D domain, it does not imply the transformed points are uniformly distributed on the underlying 3D surface.

Prediction of the linear transformation. For each point \mathbf{x}_i , we also predict a linear transformation matrix $\mathbf{T}_i \in \mathbb{R}^{3 \times 3}$ from the local surface feature \mathbf{c}_i , i.e.,

$$\mathbf{T}_i = f_2(\mathbf{c}_i), \quad (5)$$

where $f_2(\cdot)$ denotes an MLP. Multiplying \mathbf{T}_i to the previously learned 2D samples $\{(u_i^r, v_i^r)\}_{r=1}^R$ lifts the points to the tangent plane of \mathbf{x}_i

$$\hat{\mathbf{x}}_i^r = (\hat{x}_i^r, \hat{y}_i^r, \hat{z}_i^r)^\top = \mathbf{T}_i \cdot (u_i^r, v_i^r, 0)^\top + \mathbf{x}_i. \quad (6)$$

Prediction of the coarse normal. As aforementioned, normals of points play a key role in surface reconstruction. In this module, we first estimate a coarse normal, i.e., the normal $\mathbf{n}_i \in \mathbb{R}^{3 \times 1}$ of the *tangent plane* of each input point, which are shared by all points on it. Specifically, we multiply the linear transformation matrix \mathbf{T}_i to the predefined normal $(0, 0, 1)$ which is perpendicular to the 2D parametric domain:

$$\mathbf{n}_i = \mathbf{T}_i \cdot (0, 0, 1)^\top. \quad (7)$$

3.4. Coordinate and Normal Refinement

We further refine the coarse dense point cloud $\hat{\mathcal{X}}_R = \{\hat{\mathbf{x}}_i^r\}_{i,r=1}^{M,R}$ and normals $\mathcal{N} = \{\mathbf{n}_i\}_{i=1}^M$ obtained in Sec. 3.3 by warping them to the curved 3D surface space from the tangent space, leading to \mathcal{X}_R and the accurate normals $\mathcal{N}_R = \{\mathbf{n}_i^r \in \mathbb{R}^{3 \times 1}\}_{i,r=1}^{M,R}$. Technically, we predict the z -axis offsets of the points distributed in the *tangent space* by regressing the point-wise features concatenated with their coarse coordinates, i.e.,

$$\delta_i^r = f_3(\text{Concat}(\hat{\mathbf{x}}_i^r, \mathbf{c}_i)), \quad (8)$$

where $\delta_i^r \in \mathbb{R}^1$ is the normal displacement, and $f_3(\cdot)$ stands for the process of an MLP. A typical point of the final upsampled point cloud is derived as

$$\mathbf{x}_i^r = (x_i^r, y_i^r, z_i^r)^\top = \hat{\mathbf{x}}_i^r + \mathbf{T}_i \cdot (0, 0, \delta_i^r)^\top. \quad (9)$$

The normals are refined in a similar way. Specifically, a normal offset $\Delta \mathbf{n}_i^r \in \mathbb{R}^{3 \times 1}$ for point \mathbf{x}_i^r is regressed as

$$\Delta \mathbf{n}_i^r = f_4(\text{Concat}(\hat{\mathbf{x}}_i^r, \mathbf{c}_i)), \quad (10)$$

which is further added to the corresponding coarse normal, leading to

$$\mathbf{n}_i^r = \Delta \mathbf{n}_i^r + \mathbf{n}_i, \quad (11)$$

where $f_4(\cdot)$ is the process of an MLP.

3.5. Joint Loss Optimization

As PUGeo-Net aims to deal with the regression of both coordinates and unoriented normals of points, we design a joint loss to train it end-to-end. Specifically, let $\mathcal{Y}_R = \{\mathbf{y}_k\}_{k=1}^{RM}$ with RM points be the groundtruth of \mathcal{X}_R . During training, we adopt the Chamfer distance (CD) to measure the coordinate error between the \mathcal{X}_R and \mathcal{Y}_R , i.e.,

$$L_{CD} = \frac{1}{RM} \left(\sum_{\mathbf{x}_i^r \in \mathcal{X}_R} \|\mathbf{x}_i^r - \phi(\mathbf{x}_i^r)\|_2^2 + \sum_{\mathbf{y}_k \in \mathcal{Y}_R} \|\mathbf{y}_k - \psi(\mathbf{y}_k)\|_2^2 \right), \quad (12)$$

where $\phi(\mathbf{x}_i^r) = \arg \min_{\mathbf{y}_k \in \mathcal{Y}_R} \|\mathbf{x}_i^r - \mathbf{y}_k\|_2$, $\psi(\mathbf{y}_k) = \arg \min_{\mathbf{x}_i^r \in \mathcal{X}_R} \|\mathbf{x}_i^r - \mathbf{y}_k\|_2$, and $\|\cdot\|_2$ is the ℓ_2 norm of a vector.

For the normal part, denote $\tilde{\mathcal{N}} = \{\tilde{\mathbf{n}}_i\}_{i=1}^M$ and $\bar{\mathcal{N}}_R = \{\bar{\mathbf{n}}_k\}_{k=1}^{RM}$ the ground truth of the coarse normal \mathcal{N} and the accurate normal \mathcal{N}_R , respectively. During training, we consider the errors between \mathcal{N} and $\tilde{\mathcal{N}}$ and between \mathcal{N}_R and $\bar{\mathcal{N}}_R$ simultaneously, i.e.,

$$L_{coarse}(\mathcal{N}, \tilde{\mathcal{N}}) = \sum_{i=1}^M L(\mathbf{n}_i, \tilde{\mathbf{n}}_i), \quad (13)$$

$$L_{refined}(\mathcal{N}_R, \bar{\mathcal{N}}_R) = \sum_{i=1}^M \sum_{r=1}^R L(\mathbf{n}_i^r, \bar{\mathbf{n}}_{\phi(\mathbf{x}_i^r)}), \quad (14)$$

where $L(\mathbf{n}_i, \tilde{\mathbf{n}}_i) = \max\{\|\tilde{\mathbf{n}}_i - \mathbf{n}_i\|_2, \|\mathbf{n}_i + \tilde{\mathbf{n}}_i\|_2\}$ measures the unoriented difference between two normals, and $\phi(\cdot)$ is used to build the unknown correspondence between \mathcal{N}_R and $\bar{\mathcal{N}}_R$. Finally, the joint loss function is written as

$$L_{total} = \alpha L_{CD} + \beta L_{coarse} + \gamma L_{refined}, \quad (15)$$

where α , β , and γ are three positive parameters. It is worth noting that our method does not require repulsion loss which is required by PU-Net and EC-Net, since the module for learning the parametric domain is capable of densifying point clouds with uniform distribution.

Table 1: Results of quantitative comparisons. The models were scaled uniformly in a unit cube, so the error metrics are unitless. Here, the values are the average of 13 testing models. See the *Supplementary Material* for the results of each model.

R	Method	Network size	CD (10^{-2})	HD (10^{-2})	JSD (10^{-2})	P2F mean (10^{-3})	P2F std (10^{-3})	surface CD (10^{-2})	HD (10^{-2})	JSD (10^{-2})
4×	EAR [23]	-	0.919	5.414	4.047	3.672	5.592	1.022	6.753	7.445
	PU-Net [24]	10.1 MB	0.658	1.003	0.950	1.532	1.215	0.648	5.850	4.264
	MPU [26]	92.5 MB	0.573	1.073	0.614	0.808	0.809	0.647	5.493	4.259
	PUGeo-Net	26.6 MB	0.558	0.934	0.444	0.617	0.714	0.639	5.471	3.928
8×	EAR [23]	-	-	-	-	-	-	-	-	-
	PU-Net [24]	14.9 MB	0.549	1.314	1.087	1.822	1.427	0.594	5.770	3.847
	MPU [26]	92.5 MB	0.447	1.222	0.511	0.956	0.972	0.593	5.723	3.754
	PUGeo-Net	26.6 MB	0.419	0.998	0.354	0.647	0.752	0.549	5.232	3.465
12×	EAR [23]	-	-	-	-	-	-	-	-	-
	PU-Net [24]	19.7 MB	0.434	0.960	0.663	1.298	1.139	0.573	6.056	3.811
	MPU [26]	-	-	-	-	-	-	-	-	-
	PUGeo-Net	26.7 MB	0.362	0.978	0.325	0.663	0.744	0.533	5.255	3.322
16×	EAR [23]	-	-	-	-	-	-	-	-	-
	PU-Net [24]	24.5 MB	0.482	1.457	1.165	2.092	1.659	0.588	6.330	3.744
	MPU [26]	92.5 MB	0.344	1.355	0.478	0.926	1.029	0.573	5.923	3.630
	PUGeo-Net	26.7 MB	0.323	1.011	0.357	0.694	0.808	0.524	5.267	3.279

Table 2: Verification of the effectiveness of our normal prediction. Here, the upsampling ratio R is 8. PCA* indicates the normal prediction by PCA with various numbers of neighborhoods.

Methods	CD	HD	JSD
PCA-10	0.586	5.837	3.903
PCA-15	0.577	5.893	3.789
PCA-25	0.575	5.823	3.668
PCA-35	0.553	5.457	3.502
PCA-45	0.568	5.746	3.673
PU-Net-M	0.678	6.002	4.139
PUGeo-Net	0.549	5.232	3.464

4. Experimental Results

4.1. Experiment Settings

Datasets. Analogy to previous works, we selected 90 high-resolution 3D mesh models from Sketchfab [1] to construct the training dataset and 13 for the testing dataset. Specifically, given the 3D meshes, we employed the Poisson disk sampling [49] to generate \mathcal{X} , \mathcal{Y}_R , $\tilde{\mathcal{N}}$, and $\bar{\mathcal{N}}$ with $M = 5000$ and $R = 4, 8, 12$ and 16 . A point cloud was randomly cropped into patches each of $N = 256$ points. Data augmentations, including random scaling, rotation and point perturbation were also used. Note that normals are not needed during testing.

Implementation details. We empirically set the values of the three parameters α , β , and γ in the joint loss function to 100, 1, and 1, respectively. We used the Adam algorithm with the learning rate equal to 0.001. We trained the network with the mini-batch of size 8 for 800 epochs via the TensorFlow platform. *The code will be publicly available*

later.

Evaluation metrics. To quantitatively evaluate the performance of different methods, we considered four commonly-used evaluation metrics, i.e., Chamfer distance (CD), Hausdorff distance (HD), point-to-surface distance (P2F), and Jensen-Shannon divergence (JSD). For these four metrics, the lower, the better.

We also propose a new approach to quantitatively measure the quality of the generated point clouds. Instead of conducting the comparison between the generated point clouds and the corresponding groundtruth ones directly, we first performed surface reconstruction [50]. For the methods that cannot generate normals principal component analysis (PCA) was adopted to predict normals. Then we densely sampled 200,000 points from reconstructed surface. CD, HD and JSD between the densely sampled points from reconstructed surface and the groundtruth mesh were finally computed for measuring the surface reconstruction quality.

4.2. Comparison with State-of-the-art

We compared PUGeo-Net with three methods, i.e., optimization based EAR [23], and two state-of-the-art deep learning based methods, i.e., PU-Net [24] and MPU [26]. For fair comparisons, we retrained PU-Net and MPU with the same dataset as ours. Notice that EAR fails to process the task with R greater than 4, due to the huge memory consumption, and MPU can work only for tasks with R in the powers of 2, due to its natural cascaded structure. *Note that the primary EAR, PU-Net and MPU cannot predict normals.*

Quantitative comparisons. Table 1 shows the average result of 13 testing models, where we can observe that PUGeo-Net can achieve the best performance for *all*

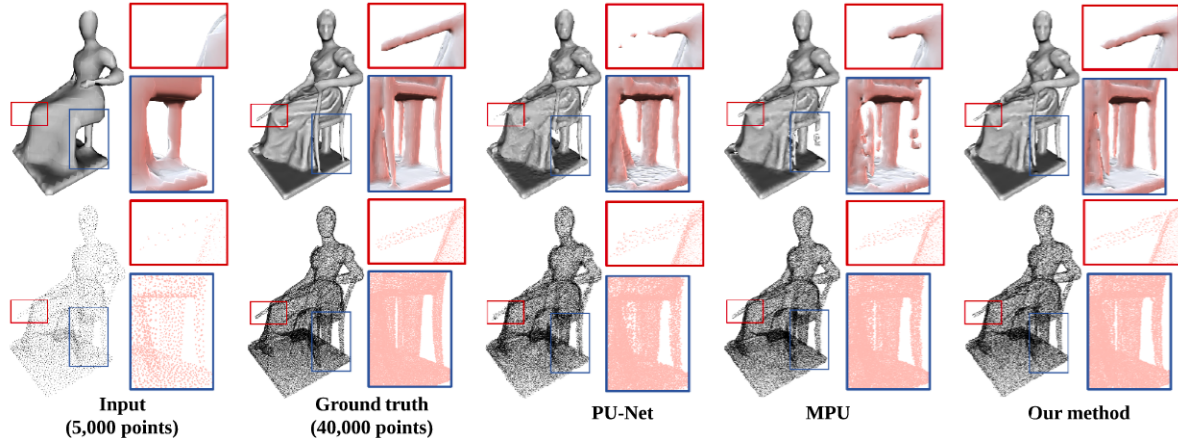


Figure 4: Visual comparisons for scanned 3D models. Each input sparse 3D point cloud has $M = 5000$ points and upsampled by a factor $R = 8$. We applied the same surface reconstruction algorithm to the sparse and densified points by different methods. For each data, the top and bottom rows correspond to the reconstructed surfaces and point clouds, respectively. As the close-up views, PUGeo-Net can handle the geometric details well. See the *Supplementary file* for more visual comparisons and the video demo.

upsample factors in terms of *all* metrics. Moreover, the network size of PUGeo-Net is fixed and much smaller than that of MPU. Due to the deficiency of the independent multi-branch design, the network size of PU-Net grows linearly with the the upsample factor increasing, and is comparable to ours when $R = 16$.

Visual comparisons. The superiority of PUGeo-Net is also visually demonstrated. We compared the reconstructed surfaces from the input sparse point clouds and the generated dense point clouds by different methods. Note that the surfaces were reconstructed via the same method [50]. Here we took the task with $R = 8$ as an example. Some parts highlighted in red and blue boxes are zoomed in for a close look. From Fig. 4, it can be observed that after performing upsampling the surfaces by PUGeo-Net present more geometric details and the best geometry structures, especially for the highly detailed parts with complex geometry, and they are closest to the groundtruth ones. We also evaluated different methods on some man-made toy models. Compared with complex statue models, these man-made models consist of flat surfaces and sharp edges, which require high quality normals for surface reconstruction. As illustrated in Fig. 5, owing to the accurate normal estimation, PUGeo-Net can preserve the flatness and sharpness of the surfaces better than PU-Net and MPU. We further investigated how the quality of the reconstructed surface by PUGeo-Net changes with the upsample factor increasing. In Fig. 1, it can be seen that as the upsample factor increases, PUGeo-Net can generate more uniformly distributed points, and the reconstructed surface is able to recover more details gradually to approach the groundtruth surface. See the *supplementary material for more visual results and the video demo*.

Comparison of the distribution of generated points.

In Fig. 6, we visualized a point cloud patch which was upsampled with 16 times by different methods. As PUGeo-Net captures the local structure of a point cloud elegantly in a geometry-centric manner, such that the upsampled points are uniformly distributed in the form of clusters. Using PUGeo-Net, the points generated from the same source point \mathbf{x}_i are uniformly distributed in a local neighborhood \mathbf{x}_i , which justifies our parameterization-based sampling strategy. PU-Net and MPU do not have such a feature. We also observe that our generated points are more uniform than theirs both locally and globally.

4.3. Effectiveness of Normal Prediction

Our proposed PUGeo-Net is the *first* deep learning based method, which can regress the coordinates and normals of points simultaneously. Here we evaluated the effectiveness of our normal prediction module by applying the predicted normals on surface reconstruction. We compared with the reconstructed surfaces with the normals predicted by PCA with various numbers of neighborhoods, ranging from 10 to 45. CD, HD, and JSD between the reconstructed surfaces from point clouds and the groundtruth ones were computed. Moreover, we also modified PU-Net, denoted as PU-Net-M, to predict coordinates and normals jointly by changing the neuron number of the last layer to 6 from 3. PU-Net-M was trained with the same training dataset as ours.

The quantitative results are shown in Table 2, where we can see that (1) the surfaces reconstructed with the normals by PUGeo-Net produces the smallest errors for all the three metrics; (2) the number of neighborhoods in PCA based normal prediction is a heuristic parameter and influences the final surface quality seriously; and (3) the PU-Net-M achieves the worst performance, indicating that a naive design without considering the geometry characteristics does not make sense.

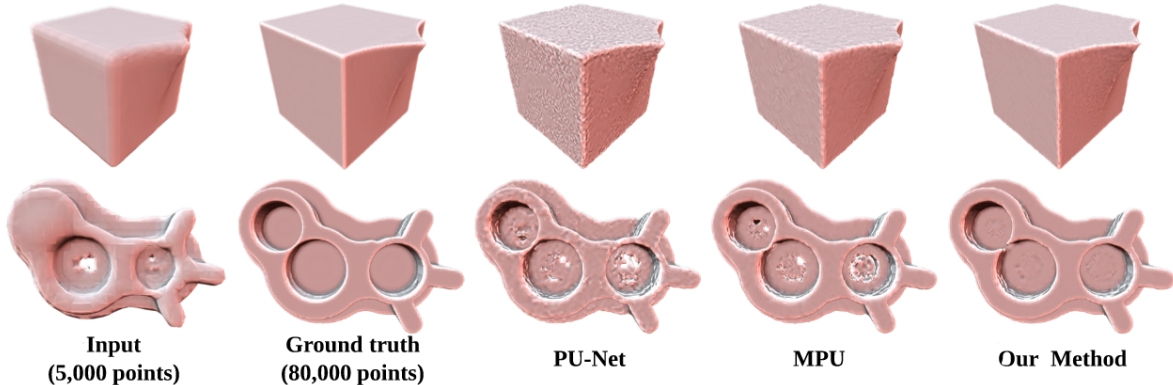


Figure 5: Visual comparisons on CAD models with the upsampling factor $R = 16$. The input point clouds have 5,000 points. We show the surfaces generated using the screened Poisson surface reconstruction (SPSR) algorithm [50]. Due to the low-resolution of the input, SPSR fails to reconstruct the geometry. After upsampling, we observe that the geometric and topological features are well preserved in our results.

Table 3: Ablation study. **Feature recalibration**: concatenate multiscale feature directly without the recalibration module. **Normal prediction**: only regress coordinates of points without normal prediction and supervision. **Learned adaptive 2D sampling**: use a predefined 2D regular grid as the parametric domain instead of the learned adaptive 2D smapling. **Linear transformation**: regress coordinates and normals by non-linear MLPs directly without prediction of the linear transformation. **Coarse to fine**: directly regress coordinates and normals without the intermediate coarse prediction.

Networks	CD	HD	JSD	P2F mean	P2F std	surface CD	HD	JSD
Feature recalibration	0.325	1.016	0.371	0.725	0.802	0.542	5.654	3.425
Normal prediction	0.331	2.232	0.427	0.785	0.973	0.563	5.884	3.565
Learned adaptive 2D sampling	0.326	1.374	0.407	0.701	0.811	0.552	5.758	3.456
Linear transformation	0.394	1.005	1.627	0.719	0.720	1.855	11.479	9.841
Coarse to fine	0.330	1.087	0.431	0.746	0.748	0.534	5.241	3.348
Full model	0.323	1.011	0.357	0.694	0.808	0.524	5.267	3.279

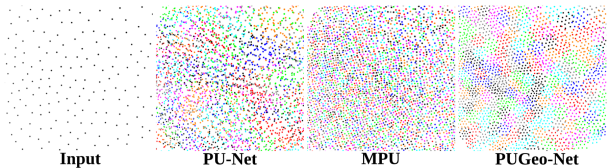


Figure 6: Visual comparison of the distribution of generated 2D points with upsampling factor $R = 16$. We distinguish the generated points by their source, assigned with colors. The points generated by PUGeo-Net are more uniform than those of PU-Net and MPU.

4.4. Ablation Study

We conducted an ablation study towards our model to evaluate the contribution and effectiveness of each module. Table 3 shows the quantitative results. Here we took the task with $R = 8$ as an example, and similar results can be observed for other upsampling factors.

From Table 3, we can conclude that (1) directly regressing the coordinates and normals of points by simply using MLPs instead of the linear transformation decreases the upsampling performance significantly, demonstrating the superiority of our geometry-centric design; (2) the joint regression of normals and coordinates are better than

that of only coordinates; and (3) the other novel modules, including feature recalibration, adaptive 2D sampling, and the coarse to fine manner, all contribute to the final performance.

5. Conclusion and Future Work

We presented PUGeo-Net, a novel deep learning based framework for 3D point cloud upsampling. As the first deep neural network constructed in perspective of discrete differential geometry, PUGeo-Net has many distinctive features, such as learning the best linear approximation of local surface parameterization, generating uniformly distributed points and their normals from sparse point clouds, and preserving sharp features, making it an ideal pre-processing tool for the existing surface reconstruction algorithms. Extensive evaluation shows PUGeo-Net outperforms the state-of-the-art deep learning methods for 3D point cloud upsampling in terms of accuracy and efficiency.

Thanks to its geometry-centric nature, we believe our network can be extended to other 3D point cloud processing tasks, such as point clouds resampling, denoising, and compression. We will also investigate the effectiveness of PUGeo-Net on incomplete point clouds.

References

- [1] Sketchfab,
<https://sketchfab.com>
- [2] Orts-escolano, S., Rhemann, C., Fanello, S., Chang, W., Kowdle, A., Degtyarev, Y., Kim, D., Davidson, P., Khamis, S., Dou, M. Holoportation: Virtual 3d teleportation in real-time.
- [3] Lafarge, F., Mallet, C. Creating large-scale city models from 3D-point clouds: a robust approach with hybrid representation. *International Journal Of Computer Vision*. **99**, 69–85 (2012)
- [4] Musialski, P., Wonka, P., Aliaga, D., Wimmer, M., Vangool, L., Purgathofer, W. A survey of urban reconstruction.
- [5] Xu, Z., Wu, L., Shen, Y., Li, F., Wang, Q., Wang, R. Tridimensional reconstruction applied to cultural heritage with the use of camera-equipped UAV and terrestrial laser scanner. *Remote Sensing*. **6**, 10413–10434 (2014)
- [6] Bolognesi, M., Furini, A., Russo, V., Pellegrinelli, A., Russo, P. TESTING THE LOW-COST RPAS POTENTIAL IN 3D CULTURAL HERITAGE RECONSTRUCTION.. *International Archives Of The Photogrammetry, Remote Sensing & Spatial Information Sciences*. (2015)
- [7] Paine, J., Caudle, T., Andrews, J. Shoreline and sand storage dynamics from annual airborne LIDAR surveys, Texas Gulf Coast. *Journal Of Coastal Research*. **33**, 487–506 (2016)
- [8] Nie, S., Wang, C., Dong, P., Xi, X., Luo, S., Zhou, H. Estimating leaf area index of maize using airborne discrete-return LiDAR data. *Ieee Journal Of Selected Topics In Applied Earth Observations And Remote Sensing*. **9**, 3259–3266 (2016)
- [9] Chen, X., Ma, H., Wan, J., Li, B., Xia, T. Multi-view 3d object detection network for autonomous driving.
- [10] Li, B. 3d fully convolutional network for vehicle detection in point cloud.
- [11] Fioraio, N., Konolige, K. Realtime visual and point cloud slam.
- [12] Cole, D., Newman, P. Using laser range data for 3D SLAM in outdoor environments.
- [13] Held, R., Gupta, A., Curless, B., Agrawala, M. 3D puppetry: a kinect-based interface for 3D animation..
- [14] Santana, J., Wendel, J., Trujillo, A., Suárez, J., Simons, A., Koch, A. Multimodal location based servicesemantic 3D city data as virtual and augmented reality. (Springer,2017)
- [15] Hakala, T., Suomalainen, J., Kaasalainen, S., Chen, Y. Full waveform hyperspectral LiDAR for terrestrial laser scanning. *Optics Express*. **20**, 7119–7127 (2012)
- [16] Kimoto, K., Asada, N., Mori, T., Hara, Y., Ohya, A. Development of small size 3D LIDAR.
- [17] Lai, W., Huang, J., Ahuja, N., Yang, M. Deep laplacian pyramid networks for fast and accurate super-resolution.
- [18] Zhang, Y., Tian, Y., Kong, Y., Zhong, B., Fu, Y. Residual dense network for image super-resolution.
- [19] Alexa, M., Behr, J., Cohen-or, D., Fleishman, S., Levin, D., Silva, C. Computing and rendering point set surfaces. *Ieee Transactions On Visualization And Computer Graphics*. **9**, 3–15 (2003)
- [20] Lipman, Y., Cohen-or, D., Levin, D., Tal-ezer, H. Parameterization-free projection for geometry reconstruction.
- [21] Huang, H., Li, D., Zhang, H., Ascher, U., Cohen-or, D. Consolidation of unorganized point clouds for surface reconstruction. *Acm Transactions On Graphics (tog)*. **28**, 176 (2009)
- [22] Preiner, R., Mattausch, O., Arikian, M., Pajarola, R., Wimmer, M. Continuous projection for fast L1 reconstruction.. *Acm Transactions On Graphics (tog)*. **33**, 47–1 (201)
- [23] Huang, H., Wu, S., Gong, M., Cohen-or, D., Ascher, U., Zhang, H. Edge-aware point set resampling. *Acm Transactions On Graphics (tog)*. **32**, 9 (2013)
- [24] Yu, L., Li, X., Fu, C., Cohen-or, D., Heng, P. Pu-net: Point cloud upsampling network.
- [25] Yu, L., Li, X., Fu, C., Cohen-or, D., Heng, P. EC-Net: an Edge-aware Point set Consolidation Network.
- [26] Wang, Y., Wu, S., Huang, H., Cohen-or, D., Sorkinehornung, O. Patch-based Progressive 3D Point Set Upsampling.
- [27] Qi, C., Yi, L., Su, H., Guibas, L. Pointnet++: Deep hierarchical feature learning on point sets in a metric space.
- [28] Maturana, D., Scherer, S. Voxnet: A 3d convolutional neural network for real-time object recognition.

- [29] Riegler, G., Osmanulusoy, A., Geiger, A. Octnet: Learning deep 3d representations at high resolutions.
- [30] Wu, Z., Song, S., Khosla, A., Yu, F., Zhang, L., Tang, X., Xiao, J. 3d shapenets: A deep representation for volumetric shapes.
- [31] Rieu, L., Simonovsky, M. Large-scale point cloud semantic segmentation with superpoint graphs.
- [32] Te, G., Hu, W., Zheng, A., Guo, Z. Rgcnn: Regularized graph cnn for point cloud segmentation.
- [33] Qi, C., Su, H., Mo, K., Guibas, L. Pointnet: Deep learning on point sets for 3d classification and segmentation.
- [34] Wang, Y., Sun, Y., Liu, Z., Sarma, S., Bronstein, M., Solomon, J. Dynamic graph cnn for learning on point clouds. *Acm Transactions On Graphics (tog)*. **38**, 146 (2019)
- [35] Komarichev, A., Zhong, Z., Hua, J. A-CNN: Annularly Convolutional Neural Networks on Point Clouds.
- [36] Li, Y., Bu, R., Sun, M., Wu, W., Di, X., Chen, B. Pointcnn: Convolution on x-transformed points.
- [37] Campen, M., Bommers, D., Kobbelt, L. Quantized Global Parametrization. *Acm Transactions On Graphics (tog)*. **34**, 192:1–192:12 (2015)
- [38] Hormann, K., Greiner, G. MIPS: An Efficient Global Parametrization Method. *Curve And Surface Design: Saint-mal*. **2000** pp. 10 (2012)
- [39] Xianfeng, G., Shingtung, Y. Global Conformal Parameterization.
- [40] Jaderberg, M., Simonyan, K., Zisserman, A. Spatial transformer networks.
- [41] Ronneberger, O., Fischer, P., Brox, T. U-net: Convolutional networks for biomedical image segmentation.
- [42] He, K., Zhang, X., Ren, S., Sun, J. Deep residual learning for image recognition.
- [43] Huang, G., Liu, Z., Vandermaaten, L., Weinberger, K. Densely connected convolutional networks.
- [44] Hu, J., Shen, L., Sun, G. Squeeze-and-excitation networks.
- [45] Zhang, H., Goodfellow, I., Metaxas, D., Odena, A. Self-Attention Generative Adversarial Networks.
- [46] Yang, Y., Feng, C., Shen, Y., Tian, D. Foldingnet: Point cloud auto-encoder via deep grid deformation.
- [47] Deng, H., Birdal, T., Ilic, S. Ppfnet: Global context aware local features for robust 3d point matching.
- [48] Yuan, W., Khot, T., Held, D., Mertz, C., Hebert, M. Pcn: Point completion network.
- [49] Corsini, M., Cignoni, P., Scopigno, R. Efficient and flexible sampling with blue noise properties of triangular meshes. *Ieee Transactions On Visualization And Computer Graphics*. **18**, 914–924 (2012)
- [50] Kazhdan, M., Hoppe, H. Screened poisson surface reconstruction. *Acm Transactions On Graphics (tog)*. **32**, 29 (2013)